3-9-2012

Observed and Modeled Solar Cycle Variation in Geocoronal Hydrogen Using NRLMSISE-00 Thermosphere Conditions and the Bishop Analytic Exosphere Model

S. M. Nossal
University of Wisconsin - Madison

E. J. Mierkiewicz
University of Wisconsin - Madison, mierkiee@erau.edu

F. L. Roesler
University of Wisconsin - Madison

Observed and modeled solar cycle variation in geocoronal hydrogen using NRLMSISE-00 thermosphere conditions and the Bishop analytic exosphere model

S. M. Nossal,[1] E. J. Mierkiewicz,[1] and F. L. Roesler[1]

Received 16 August 2011; revised 1 December 2011; accepted 12 January 2012; published 9 March 2012.

[1] High precision observations during Solar Cycle 23 using the Wisconsin H-alpha Mapper (WHAM) Fabry-Perot quantify a factor of 1.5 ± 0.15 higher Balmer α column emission intensity during near-solar-maximum than during solar minimum conditions. An unresolved question is how does the observed solar cycle variation in the hydrogen column emission compare with that calculated from the hydrogen distribution in atmospheric models? We have compared WHAM solar minimum and near-solar-maximum column intensity observations with calculations using the thermospheric hydrogen density profile and background thermospheric conditions from the Mass Spectrometer Incoherent Scatter (NRLMSISE-00) empirical model extended to exospheric altitudes using the analytic exosphere model of Bishop (1991). Using this distribution, we apply the lyao_rt global resonance radiative transfer code of Bishop (1999) to calculate expected intensities that would be observed from the ground for the viewing conditions of the observations. The observed intensities are brighter than those calculated for the corresponding conditions, indicating that when MSIS is used as the thermospheric hydrogen distribution the derived intensities are too low. Additionally, both the observed and calculated WHAM hydrogen column emission intensities are higher for near-solar-maximum than for solar minimum conditions. There is better agreement between observations and intensities calculated using the evaporative analytic exosphere model at solar maximum, suggesting an underestimation of modeled satellite atoms at high altitudes. This result is consistent with sensitivity studies using the option for a quasi-exobase for satellite atoms to account for the creation of satellite orbits from charge exchange collisions.

Citation: Nossal, S. M., E. J. Mierkiewicz, and F. L. Roesler (2012), Observed and modeled solar cycle variation in geocoronal hydrogen using NRLMSISE-00 thermosphere conditions and the Bishop analytic exosphere model, *J. Geophys. Res.*, *117*, A03311, doi:10.1029/2011JA017074.

1. Introduction

[2] Hydrogen is a key constituent of the thermosphere and exosphere and is a byproduct of chemical and physical processes lower in the atmosphere that involve important radiative species such as methane and water vapor [*Brasseur and Solomon*, 2005]. Geocoronal hydrogen is more globally mixed than are hydrogen-containing species at lower altitudes because of its long mean free paths and orbital dynamics [*Chamberlain and Hunten*, 1987]. Thus, knowledge of geocoronal hydrogen is expected to contribute to understanding the hydrogen budget of the whole atmosphere system.

[3] The University of Wisconsin has acquired a long-term data set from midlatitudes consisting of high precision, consistently calibrated observations of the hydrogen Balmer α column emission. The observations are being used to investigate the impact on hydrogen of the 11-year solar cycle, a major source of natural forcing in the upper atmosphere. Knowledge of natural variability is crucial to efforts to isolate possible long-term trends in hydrogen emission observations. The Wisconsin Northern hemisphere midlatitude data set indicates a statistically significant solar cycle dependence over two solar cycles (embracing three solar minima) with column emission intensities a factor of ~1.5 ± 0.15 higher during near-solar-maximum than during solar minimum conditions [*Nossal et al.*, 2004, 2008].

[4] The solar cycle variation in the midlatitude Wisconsin and Kitt Peak observations differs from that reported from the Arecibo Observatory (18.35°N; 66.75°W) [*Kerr et al.*, 2001a, 2001b]. In contrast to the Wisconsin midlatitude observations, a solar cycle variation is only observed in the Arecibo observations for shadow altitudes less than 2000 km, and the emissions are higher during solar *minimum* conditions, opposite to the Wisconsin observations [*Kerr et al.*, 2001a]. Further comparison studies are required to determine whether these differences are geophysical or due

[1]Department of Physics, University of Wisconsin-Madison, Madison, Wisconsin, USA.

0148-0227/12/2011JA017074

to viewing geometry or other factors. An interpretation of the Arecibo observations is not addressed in this study.

[5] An unresolved question is how does the observed solar cycle variation in the hydrogen column emission compare with variation in the hydrogen distribution in atmospheric models? The Fabry-Perot measures the line-of-sight hydrogen Balmer α column emission intensity. In the geocorona, the hydrogen Balmer α emission line is primarily excited by the line center of the solar Lyman β emission. Systematic model validation with long-term geocoronal column emission data sets is thus challenging because the observed emissions depend on the hydrogen density distribution, the solar excitation flux, and radiative transfer, including multiple scattering of the solar Lyman β excitation radiation below the Earth's shadow.

[6] In this paper we present a validation approach using the lyao_rt nonisothermal atomic resonance radiative transfer code of *Bishop* [1999] to facilitate initial comparisons between our midlatitude long timeline Balmer α column emission observations and the Mass Spectrometer Incoherent Scatter (NRLMSISE-00) empirical model [*Picone et al.*, 2002; *Hedin*, 1991] extended to exospheric altitudes with the analytic model of *Bishop* [1991]. We use the lyao_rt code with this hydrogen density profile to calculate intensities corresponding to the viewing geometry of our observations. We chose the NRLMSISE-00 model because of its frequent use for comparisons with observations. In the future, we plan to apply the technique used here for validation of other existing models and in support of model development efforts extending to exospheric altitudes.

2. Wisconsin Long Timeline Observational Data Set

[7] The University of Wisconsin has observed geocoronal hydrogen Balmer α emissions since the late 1970s from Wisconsin (43.07°N; 270.33°E), and during Solar Cycle 23 from Kitt Peak, Arizona (31.98°N; 248.40°E) with the Wisconsin H-alpha Mapper (WHAM) Fabry-Perot [*Nossal et al.*, 2001, 2008; *Haffner et al.*, 2003]. These observations were all obtained using ground-based double etalon Fabry-Perot Interferometers with sufficient resolution ($\sim$80,000 and $\sim$25,000) to differentiate geocoronal from Galactic Balmer α emission [*Mierkiewicz et al.*, 2006; *Nossal et al.*, 2006; *Haffner et al.*, 2003]. Earlier observations used scanning photomultiplier detection, and the Solar Cycle 23 observations employed CCD annular summing spectroscopy [*Reynolds et al.*, 1990; *Coakley et al.*, 1996]. Tracking siderostats allowed all of the observations to be calibrated using Balmer α emission nebulae, all tied to the absolute intensity calibration of the North American Nebula (NGC7000) [*Scherb*, 1981; *Nossal et al.*, 2008]. The precision of the observations has increased over time as the instrumental sensitivity has been improved.

[8] High precision observations of the geocoronal hydrogen Balmer α emission by WHAM during solar minimum and near-solar-maximum conditions are plotted versus shadow altitude in Figure 1. The shadow altitude is the viewing geometry parameter with the greatest impact on the column emission intensity. Solar Lyman β is fully absorbed by atmospheric O_2 below 102 km. Thus, for Lyman β excitation the Earth's shadow forms a cylinder with a radius that is 102 km greater than that of the Earth. The shadow altitude is the altitude of the location where the observational line of sight intersects this cylinder. The observed emission arises primarily from hydrogen at the base of the illuminated column because the hydrogen density falls off with altitude. Multiple scattering of solar Lyman β below the Earth's shadow also contributes to the column emission intensity and becomes an increasing fraction of the intensity at larger shadow altitudes. For a given shadow altitude, there can be differences in intensity within approximately 1 Rayleigh, due to differences in slant path through the atmosphere corresponding to differences in the zenith angle of the observation [*Nossal et al.*, 2001].

[9] The observations used for the WHAM solar cycle study were taken during moonless, clear sky conditions during winter months (December–March) when sky conditions are typically best, and were pointed toward very low Galactic emission regions ($\leq$0.6 Rayleighs). The observational zenith angle was less than 50 degrees to reduce uncertainties due to tropospheric scattering. The observations presented here are from 22 nights of exceptional viewing quality. For the near-solar-maximum observations (within a year of solar maximum), the F10.7 cm radio flux index ranged from 134 to 163 and the conditions were geomagnetically quiet with an Ap index ranging from 4 to 11. For the solar minimum observations, the F10.7 index ranged from 69 to 77, with Ap ranging from 2 to 9, with one day having an Ap index of 22. There is a $\pm$ 10% uncertainty in the relative calibration of these observations and hence of the comparison between the solar minimum and near-solar-maximum WHAM observed intensities. Detailed information about the observations, calibration, and assessment of uncertainty is included in work by *Nossal et al.* [2008].

[10] Analysis of observations from the Wisconsin H-alpha Mapper during Solar Cycle 23 indicates a statistically significant solar cycle dependence. As shown in Figure 1, observations from the 1997 and the 2006–2008 minima are consistent, showing intensities near-solar-maximum to be higher than those at solar minimum for all shadow altitudes [*Nossal et al.*, 2008]. The WHAM Balmer α column emission intensity is a factor of $\sim$1.5 $\pm$ 0.15 higher during near-solar-maximum conditions. When *Nossal et al.* [2008] corrected the WHAM solar cycle observations using the tropospheric scattering estimation code of *Leen* [1979], the ratio between the near-solar-maximum and solar minimum column emission intensities remained close to 1.5. The observations presented in Figure 1 are corrected for extinction, but not for tropospheric scattering, pending completion of an updated tropospheric scattering correction code. The WHAM observations corroborate evidence of a solar cycle variation in the less accurate Solar Cycle 22 observations taken at the Pine Bluff, Wisconsin observatory [*Nossal et al.*, 1993, 2008].

3. Lyao_rt Global Resonance Radiative Transfer Code

[11] The lyao_rt global resonance radiative transfer code [*Bishop*, 1999] was used by *Bishop* [2001] and *Bishop et al.* [2001, 2004] to facilitate detailed data/forward modeling comparisons using satellite Lyman α [*Bishop*, 2001] and

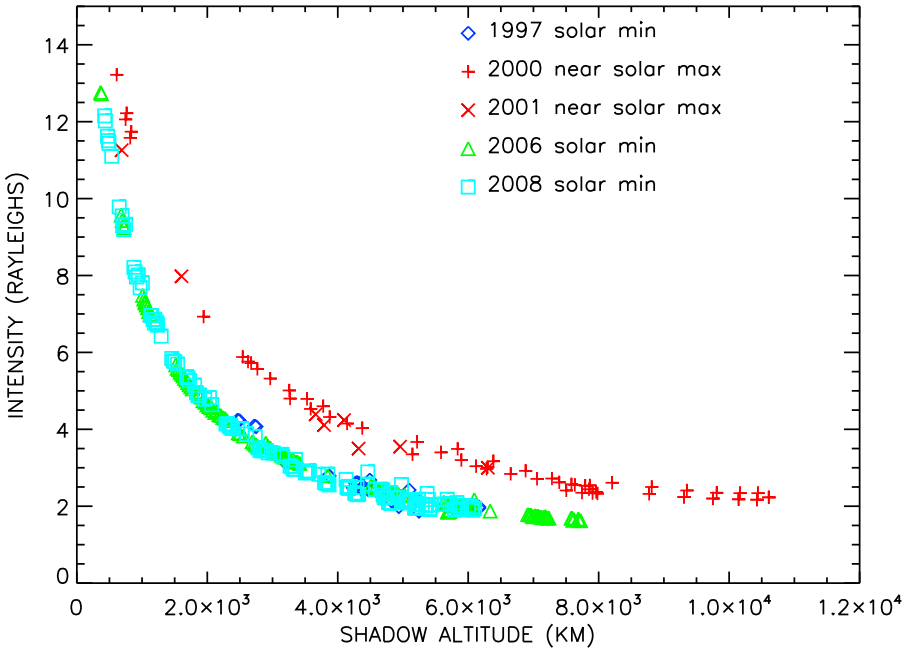

Figure 1. Observations by the Wisconsin H-alpha Mapper Fabry-Perot (WHAM) of the geocoronal hydrogen Balmer α (656.3 nm) column emission plotted versus shadow altitude. The observations are those pointed toward very low Galactic emission regions of the sky and were taken during winter, clear sky, and moonless nights. The data in this figure are from 22 nights of exceptional viewing quality. For the near-solar-maximum observations, the F10.7 index ranged from 134 to 163 and the conditions were geomagnetically quiet with an Ap index ranging from 4 to 11. For the solar minimum observations, the F10.7 index ranged from 69 to 77, with Ap ranging from 2 to 9, with one day having an Ap index of 22. The uncertainty in the *relative* intensity of the displayed WHAM observations is $\pm$ 10%. Further details about the observations are found in the text and in work by *Nossal et al.* [2008].

ground-based Fabry-Perot Balmer α observations. *Bishop et al.* [2001] used sequences of observations with multiple viewing geometries and *Bishop et al.* [2004] used near coincident ground-based Balmer α and satellite Lyman β observations as multiemission line constraints to retrieve geophysical information such as the hydrogen column abundance and upward flux from the mesosphere. The lyao_rt code can also be used to discern whether an observed variation in intensity is due to viewing geometry differences [*Nossal et al.*, 2001].

[12] Here we use the lyao_rt code as a tool to assist us in comparing the solar cycle variation in our long-term record of Fabry-Perot Balmer α emissions with the variation in modeled hydrogen distributions. We use the lyao_rt code to calculate the expected column emission intensity that would be observed from the ground corresponding to the modeled hydrogen distribution. This is done by coupling the lyao_rt code to the NRLMSISE-00 model, using both the background atmospheric conditions and the thermospheric hydrogen density profile directly from MSIS. The hydrogen density profile is extended upward using the analytic exospheric model of *Bishop* [1991].

[13] The lyao_rt code accounts for non-isothermal conditions and multiple as well as single scattering excitation by solar Lyman emissions in a spherically symmetric geometric framework [*Bishop*, 1999]. The observational and solar zenith angles and the relative azimuth between the observational and solar directions are used by the lyao_rt code to determine the Balmer α column emission intensities that would be observed from the ground for a given modeled hydrogen density profile.

4. Hydrogen Distributions From NRLMSISE-00 With the Bishop Analytic Exospheric Model Extension

[14] The Mass Spectrometer Incoherent Scatter Model (NRLMSISE-00) is an empirical model extending from the ground to the exobase and is commonly used as a standard for data/model comparisons [*Picone et al.*, 2002; *Hedin*, 1991]. Thermospheric hydrogen densities in the MSIS model are derived from charge exchange equilibrium analyses of Atmospheric Explorer satellite simultaneous observations of H^+, O^+, and O. These observations are mostly from orbits above 250 km, with the extrapolations to lower thermospheric altitudes using adjustments to a diffusive equilibrium profile [*Brinton et al.*, 1975; *Breig et al.*, 1976; *Bishop*, 2001].

[15] Figure 2a is a plot of the NRLMSISE-00 thermospheric hydrogen distribution versus altitude for morning (5 A.M. local time) conditions during solar minimum and near-solar-maximum. The distributions are for winter dates for F10.7 values of 75 and 150 and geomagnetically quiet conditions, corresponding to average values for the WHAM observations used in this study.

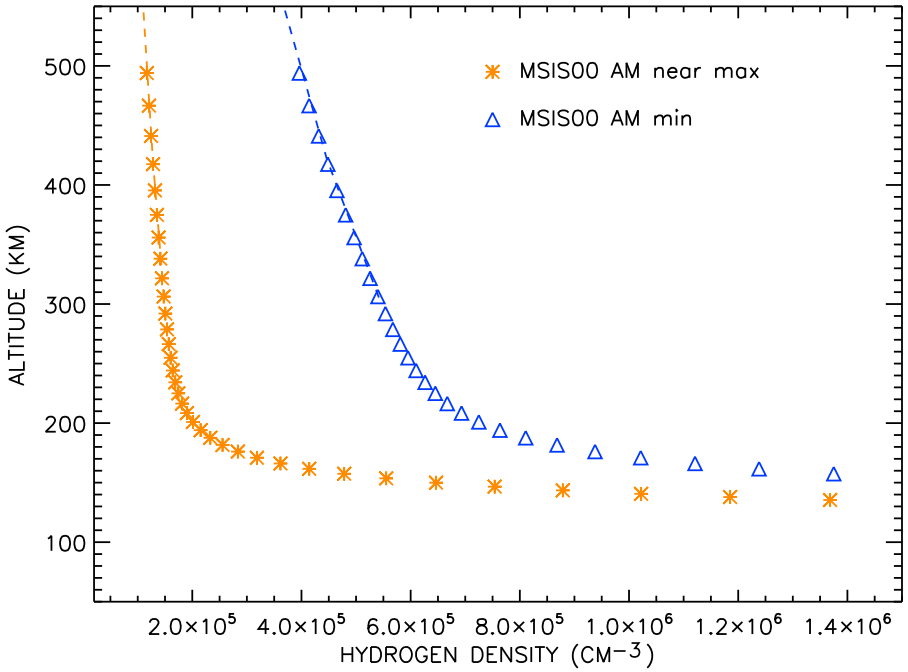

Figure 2a. Thermospheric hydrogen distributions in the Mass Spectrometer Incoherent Scatter (NRLMSISE-00) model for winter solar minimum and near-solar-maximum A.M. (5 A.M. local time) geomagnetic quiet conditions.

[16] The *Bishop* [1991] exospheric extension allows for a Chamberlain model exosphere [*Chamberlain*, 1963] or a modified Chamberlain model atmosphere specified by the analytic exosphere model of *Bishop* [1991]. The latter has the option for a satellite atom specification, accounting for the effects of charge exchange collisions with plasmaspheric

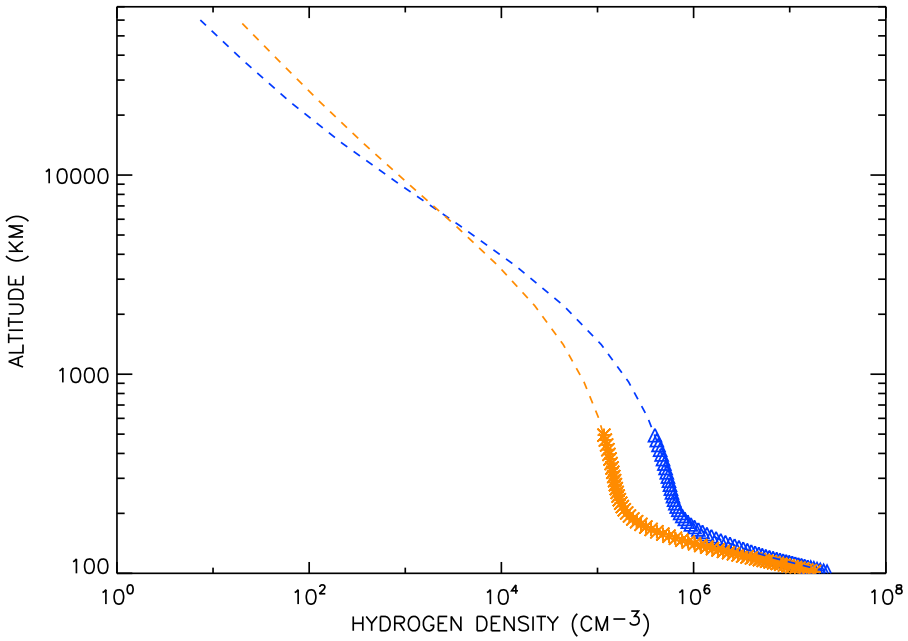

Figure 2b. Exospheric hydrogen extension using the analytic evaporative exospheric model of *Bishop* [1991]. The hydrogen density is plotted versus altitude (on log scales) for the exospheric extensions (dotted lines) of the NRLMSISE-00 thermospheric hydrogen distributions (symbols) of Figure 2a. The evaporative option of the *Bishop* [1991] analytic exospheric model was used to calculate the hydrogen profile at exospheric altitudes using exobase inputs from MSIS. The solar minimum hydrogen density profile is blue and the near-solar-maximum profile is orange.

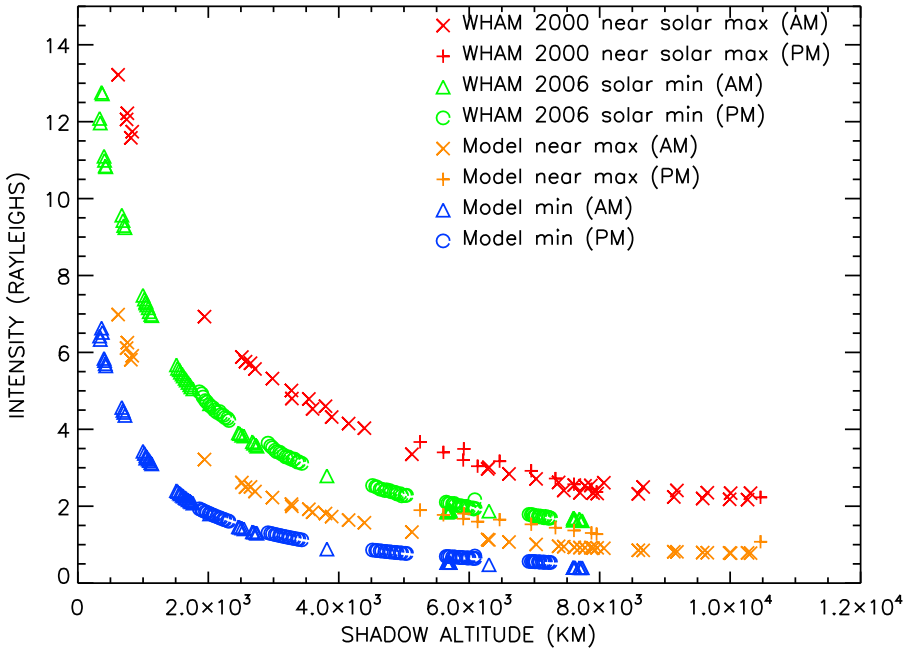

Figure 3. Hydrogen column emission intensities calculated using the lyao_rt forward model of *Bishop* [1999], the NRLMSISE-00 [*Picone et al.*, 2002] thermosphere hydrogen distribution for solar minimum and near-solar-maximum pre- and post-midnight conditions, and the analytic evaporative exospheric model extension of *Bishop* [1991]. Also included are WHAM observations taken during solar minimum and near-solar-maximum conditions. The viewing geometries used to calculate the intensities correspond to those of the WHAM observations. The A.M./P.M. asymmetries in the calculated intensities for shadow altitudes higher than about 5000 km is likely an artifact due to using a hydrogen profile calculated once for the morning and once for the evening (see text for further details).

ions [*Bishop*, 1991]. In Figure 2b, the MSIS hydrogen distribution has been extended to exospheric altitudes using the "evaporative" case of the analytic exospheric model of *Bishop* [1991, 1985]. In the "evaporative" version of the model the population of atoms on satellite orbital trajectories is characterized by the kinetic distribution of the population of atoms on ballistic trajectories, i.e., the exobase temperature and density are used as inputs to specify both the ballistic and satellite orbital populations [*Bishop*, 1991]. For this study, the upper thermospheric hydrogen density and temperature are supplied by NRLMSISE-00 and used as lower boundary inputs to calculate both the satellite and ballistic exospheric particle populations.

[17] We chose to focus this initial study on the evaporative extension of the *Bishop* [1991] analytic model because input parameters (exobase temperature and hydrogen density) directly from the NRLMSISE-00 model are used to determine all of the orbital exospheric populations. Additionally, *Bishop et al.* [2001] used the evaporative case in previous forward modeling for observations that used only single instrument observations. However, the evaporative model atmosphere does not account for the differences in temperature between the neutral atoms and plasmaspheric ions involved in charge exchange collisions.

[18] As shown in Figure 2b, when the NRLMSISE-00 model thermosphere is extended with the evaporative exospheric model, hydrogen densities are higher at solar minimum for altitudes below approximately 6000 km. Above this altitude the densities are higher during solar maximum conditions. A number of factors that influence the hydrogen density profile have a solar cycle dependence. The atomic hydrogen scale height decreases at cooler solar minimum temperatures and there is a larger source of exospheric atoms produced via charge exchange at solar minimum [*Tinsley et al.*, 1986]. There may be an underestimation of the satellite orbit population at higher shadow altitudes due to the evaporative model not accounting for the warmer ion population involved in the charge exchange collisional creation of the satellite orbital population, especially important at solar minimum [*Bishop*, 1991]. The Jean's escape process is temperature dependent and is greater at solar maximum. Additionally, atmospheric diffusion is temperature dependent.

[19] We have also conducted sensitivity studies by extending the NRLMSISE-00 thermospheric hydrogen distribution with the analytic model exospheric extension that introduces two additional "quasi-exobase" effective satellite parameters (T_s, n_s). These parameters account for differences in temperature between the ionospheric-plasmaspheric ions and the neutral hydrogen atoms involved in charge exchange collisions (see section 7).

5. Intensities Calculated Using the Lyao_rt Forward Model

[20] Figure 3 displays both observed and calculated hydrogen Balmer-α column emission intensities plotted as a function of shadow altitude. The modeled A.M. hydrogen distributions are those of Figures 2a and 2b, and the

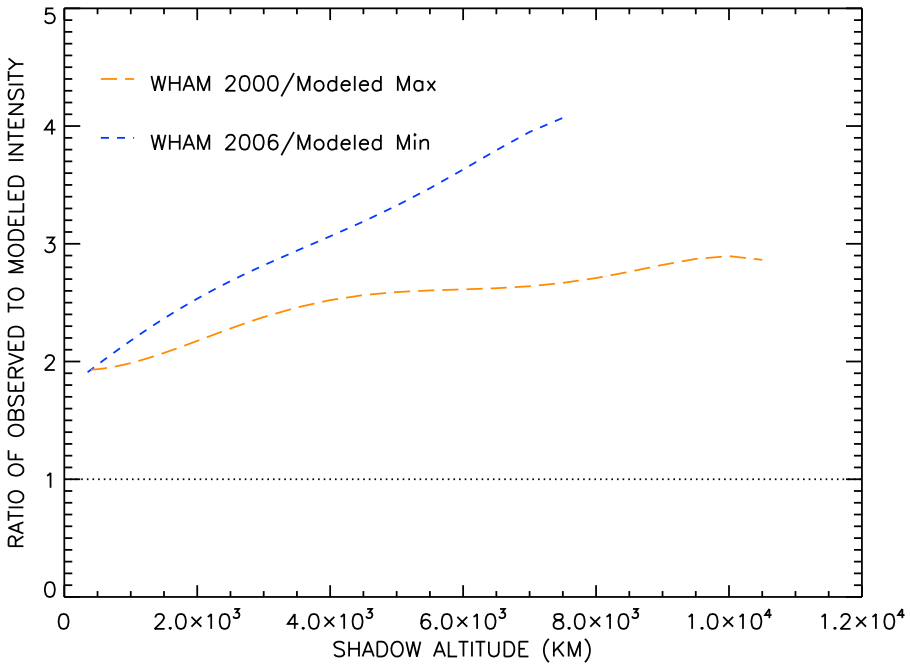

Figure 4. Ratio comparison with intensities calculated using the NRLMSISE-00 model and the *Bishop* [1991] evaporative analytic model. The observed intensity is taken in ratio to the calculated intensities of Figure 3 for A.M. hours and for solar minimum and near-solar-maximum conditions. The observed intensity is always brighter than the corresponding calculated intensity for both solar minimum and maximum conditions. Deviations from unity indicate discrepancies in the underlying hydrogen distributions. See caption of Figure 1 and text for discussion of observational uncertainties.

thermospheric temperature and background atmosphere (O_2, N_2, O) are supplied by NRLMSISE-00. The lyao_rt forward modeling global resonance radiative transfer code of *Bishop* [1999, 2001] is used to calculate the hydrogen column emission intensities that would be observed from the ground from the Kitt Peak Observatory for the modeled hydrogen distribution for the solar conditions and viewing geometries corresponding to the observations.

[21] It is the emission at the center of the solar Lyman β line that excites geocoronal hydrogen to the n = 3 level from which the Balmer α emission (n = 3 to n = 2) arises. The solar Lyman β line profile is asymmetric and self-reversed at its center [*Meier*, 1995, 1996; *Warren et al.*, 1998; *Anderson et al.*, 1987]. High-resolution observations of the solar Lyman β line are thus needed to track changes in the line center emission. High resolution solar Lyman β line profile observations from the Solar Ultraviolet Measurements of Emitted Radiation (SUMER) instrument on the Solar and Heliospheric Observatory (SOHO) satellite have been published for solar minimum and we use their measured irradiance at line center of 5×10^9 photons cm^{-2} $s^{-1}\AA^{-1}$ [*Warren et al.*, 1998]. For solar maximum conditions, we use an estimated value of 9×10^9 photons cm^{-2} $s^{-1}\AA^{-1}$ which is that used in the *Anderson et al.*, [1987] Monte Carlo radiative transfer modeling study of the ground-based geocoronal hydrogen Balmer α emission.

[22] The intensities are higher for near-solar-maximum conditions over the entire shadow altitude range for both the calculated intensities as well as for the WHAM observations. The A.M./P.M. asymmetries in the calculated intensities for shadow altitudes higher than 5000 km (see Figure 3) is likely an artifact due to using a source function calculated at UT 2 (7 P.M. local time) for the evening observations and UT12 (5 A.M. local time) for the morning observations. Our plans for future refinements to the modeling include use of a weighting of source functions to calculate midnight intensities. Although both the observed and calculated intensities are higher during solar maximum than during solar minimum conditions, there are significant differences between the calculated and observed intensities both in magnitude and in the slope of the column intensity versus shadow altitude (see Figures 3 and 4).

[23] We used fits to the observed and calculated intensities of Figure 3 to determine ratio comparisons in Figures 4 and 5. Uncertainties in the observations are described in detail by *Nossal et al.* [2008]. We fit a fifth order polynomial to the log of the intensity plotted versus shadow altitude and then used the inverse log of this polynomial as a fit to our intensities. We found that this method reduced artificial undulations in the fit arising from uneven spacing of data points with shadow altitude.

[24] In Figure 4, the fit to the observed WHAM Balmer α column emission intensities is taken in ratio to the fit of the intensities calculated with the lyao_rt code using a hydrogen distribution obtained from NRLMSISE-00 and the *Bishop* [1991] analytic evaporative exosphere model for A.M. (pre-dawn conditions). The data/model ratios at both solar minimum and near-solar-maximum differ from unity in Figure 4, indicating data/model discrepancies for the entire shadow altitude range. The calculated intensities based on the NRLMSISE-00 thermosphere and inputs to the analytic evaporative model are lower than the observations for both

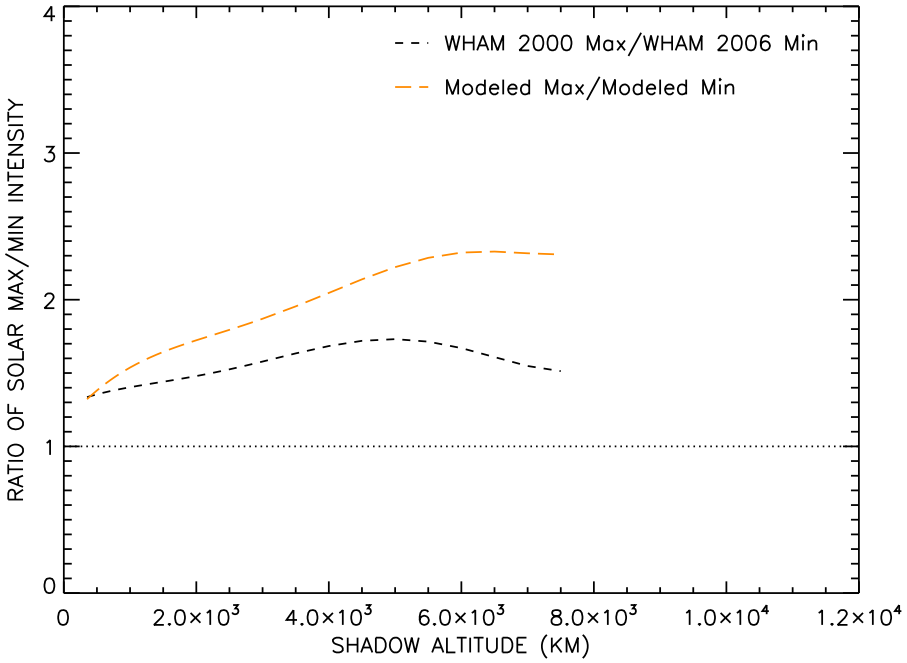

Figure 5. Ratio of near-solar-maximum to solar minimum intensities for the WHAM A.M. observations and for the calculated A.M. (pre-dawn) intensities using the lyao_rt code with the NRLMSISE-00 model thermosphere hydrogen distribution and the *Bishop* [1991] evaporative exosphere extension. The solar cycle variation in the calculated intensities is greater than that observed as indicated by the larger magnitude and slope of the ratio of the calculated maximum to minimum intensity as a function of shadow altitude. See caption of Figure 1 and text for discussion of observational uncertainties.

the solar minimum and near-solar-maximum cases and the slopes in the ratios versus shadow altitude are indicative of differences in the underlying hydrogen distributions. The agreement is better in terms of both magnitude and slope for the solar maximum case.

[25] In Figure 5 the intensities observed by WHAM during near-solar-maximum conditions are fit and taken in ratio to those observed during solar minimum conditions for morning viewing geometries. The ratios indicate that the observations are a factor of about 1.5 $\pm$ 0.15 higher during near-solar-maximum than during solar minimum conditions [*Nossal et al.*, 2008]. Similarly, the intensities calculated by the lyao_rt code for near-solar-maximum conditions for the viewing geometries corresponding to the observations are taken in ratio to those calculated for solar minimum conditions. For the calculated intensities using NRLMSISE-00 and the *Bishop* [1991] analytic evaporative exosphere model both the magnitude and slope of the solar cycle variation as a function of shadow altitude are greater than for the WHAM observations.

6. Sensitivity Study With a Constant Solar Flux

[26] In order to isolate the portion of the intensity change due to changes in the hydrogen column density from that due to the change in the solar excitation flux, we ran a sensitivity study with a constant solar Lyman-β excitation flux over the solar cycle. We used the modeled hydrogen density profile (NRLMSISE-00 plus *Bishop* [1991] analytic evaporative exosphere) used for the calculated solar minimum and near-solar-maximum intensities in Figures 3–5 and a synthetic set of zenith observing conditions to provide uniform shadow altitude coverage. We then ran the radiative transfer portion of the lyao_rt code using a solar Lyman β flux of 1×10^9 photons cm^{-2} s^{-1}Å^{-1} for both solar minimum and near-solar-maximum conditions. Figure 6 is a plot of the column emission intensity versus shadow altitude for these calculated intensities.

[27] As illustrated in Figure 6, the calculated column emission intensities (with the solar flux held constant) are brighter during solar *minimum* conditions below a shadow altitude of 1500 km. At higher shadow altitudes, the column emission intensities are brighter during solar *maximum* conditions. When keeping the solar excitation flux constant over the solar cycle, the changes in the calculated intensities are due to changes in the hydrogen column density over the solar cycle. The intensities of Figure 6 are a function of the integrated density profile, contributing to the lower crossing altitude in the column emission intensities compared with that of ~6000 km in the modeled hydrogen distributions of Figure 2b. At lower shadow altitudes the calculated column emission intensity is brighter at solar minimum for constant solar flux; however the actual solar cycle change in the solar excitation flux, along with that of the hydrogen density distribution, results in higher observed column emission intensities at solar maximum for all shadow altitudes.

7. Sensitivity Study With a Satellite Quasi-Exobase

[28] The upper atmospheric hydrogen density profile is dependent on both the model thermosphere and the

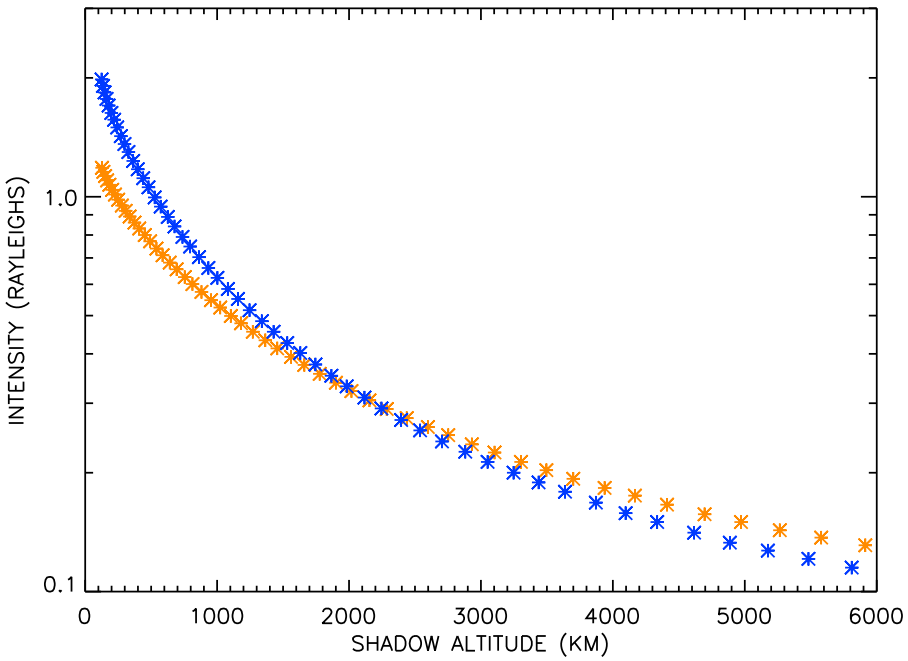

Figure 6. Sensitivity study with a constant solar Lyman-β excitation flux (1×10^9 photons cm^{-2} s^{-1}Å^{-1}) for both solar minimum (blue) and near-solar-maximum (orange) conditions and with a synthetic set of zenith observing geometries. The modeled hydrogen density profiles are the same as those used for the data/model comparisons (Figures 2–5) using the NRLMSISE-00 thermosphere and *Bishop* [1991] analytic evaporative exosphere. The column emission intensity is plotted on a log scale versus shadow altitude and indicates solar cycle differences in the hydrogen column density.

exospheric extension. We conducted sensitivity studies using the option in the *Bishop* [1991] analytic model for specification of satellite specific parameters to account for the differences in the temperatures of the ion and neutral atoms involved in charge exchange reactions. These parameters (n_s, T_s) formulate a quasi-exobase for satellite atoms produced by charge exchange collisions [*Bishop*, 1991]. For these initial sensitivity studies, we used the published satellite parameters retrieved by *Bishop* [1991] to fit the Monte Carlo hydrogen distributions of *Tinsley et al.* [1986] for solar minimum and maximum conditions. However, further investigation is required to assess the extent to which it is consistent to use satellite parameters determined independently from the NRLMSISE-00 hydrogen distribution and if there is a way to tie these parameters to thermospheric inputs.

[29] Figure 7 displays the results from our sensitivity study using the NRLMSISE-00 thermospheric conditions and the quasi-exobase satellite parameters determined from the *Bishop* [1991] fits to the Monte Carlo hydrogen distributions of *Tinsley et al.* [1986]. The ratio of the WHAM observed Balmer α column emission intensities for A.M. conditions to the calculated intensities are plotted as a function of shadow altitude, analogous to Figure 4 for the evaporative exospheric extension. The thermospheric distributions are from NRLMSISE-00 and are those in Figure 2a. The satellite parameters for solar minimum (n_s = 7×10^6 cm^{-1}; T_s = 575 K) and maximum ($n_s = 2.2 \times 10^5$ cm^{-1}; T_s = 900 K) are those retrieved by *Bishop* [1991]. The corresponding exobase parameters fit to the Monte Carlo distribution for solar minimum ($n_c = 2.4 \times 10^5$ cm^{-1}; T_c = 650 K) and maximum ($n_c = 3.6 \times 10^4$ cm^{-1}; T_s = 1250 K) differ from the corresponding NRLMSISE-00 exobase parameters used in this study for solar minimum ($n_c = 3.96 \times 10^5$ cm^{-1}; T_c = 634 K) and near-solar-maximum ($n_c = 1.167 \times 10^5$ cm^{-1}; T_c = 841 K) conditions. For this choice of satellite parameters, the densities throughout our altitude range are higher at solar minimum. The resulting calculated column emission intensities with a constant solar excitation flux are also brighter at solar minimum throughout the shadow altitude range.

[30] The use of satellite parameters to account for charge exchange results in the slopes of the observed-to-calculated intensity ratios as a function of shadow altitude being smaller for both solar minimum and maximum conditions (Figure 7) than when the evaporative exospheric extension (Figure 4) is used. The flattening of the slope is more pronounced for solar minimum than for solar maximum conditions, consistent with the greater role of charge exchange collisions in creating the satellite population at solar minimum [*Bishop*, 1991].

8. Discussion

[31] The lyao_rt global resonance radiative transfer code of *Bishop* [1999, 2001] has been used to facilitate comparisons between the solar cycle variation observed in the Wisconsin midlatitude geocoronal hydrogen column emission data set and the thermospheric hydrogen distribution in the NRLMSISE-00 model extended to exospheric altitudes with the analytic model of *Bishop* [1991]. The observed intensities are higher than those calculated for the

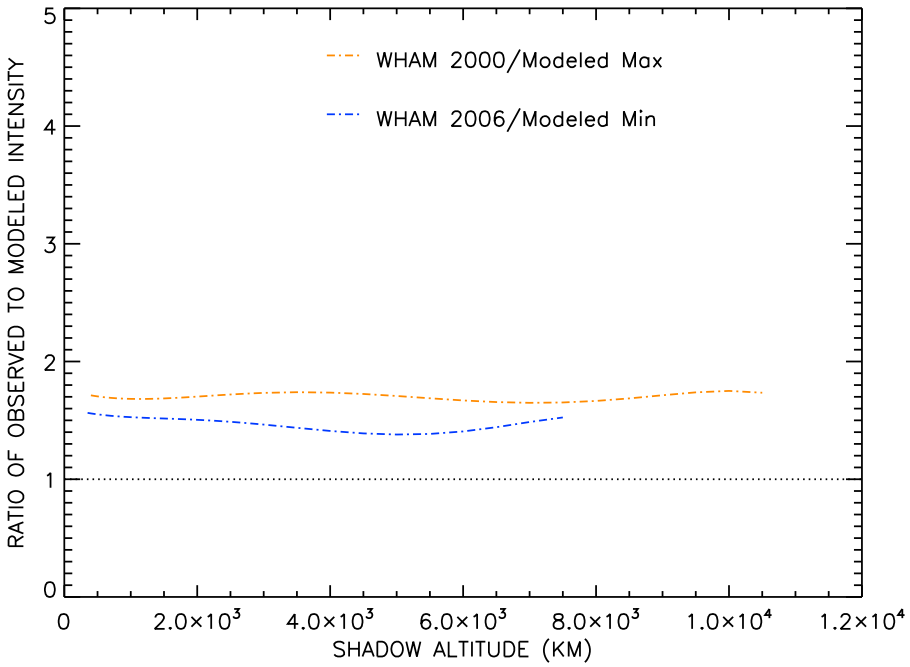

Figure 7. Ratio comparison with intensities calculated using the NRLMSISE-00 model and the *Bishop* [1991] analytic model with a quasi-exobase for satellite atoms. The observed intensity is taken in ratio to the calculated intensity using the NRLMSISE-00 model thermosphere and the *Bishop* [1991] analytic model with the option for specification of independent satellite parameters (n_s, T_s) to account for charge exchange processes [*Bishop*, 1991]. The satellite parameters are those from the *Bishop* [1991] analytic model fit to the *Tinsley et al.* [1986] Monte Carlo hydrogen distributions for solar minimum and maximum. Further investigation is required to assess the extent to which it is consistent to use satellite parameters determined independently from the NRLMSISE-00 hydrogen distribution and if there is a way to tie these parameters to thermospheric inputs. Compare with the analogous plot for the evaporative exospheric extension (Figure 4).

corresponding solar geophysical conditions (Figures 3 and 4). For the case of an evaporative exospheric extension in which all particle populations are determined using the NRLMSISE-00 exobase density and temperature, the ratios of the observed-to-calculated intensities plotted as a function of shadow altitude have nonzero slopes for both near-solar-maximum and solar minimum conditions. If the difference were due only to the Lyman β scaling factor, the ratios would be flat over the range of shadow altitudes sampled.

[32] For the case of the evaporative exospheric extension, the slope of the observed-to-calculated ratios is less during near-solar-maximum conditions than during solar minimum conditions, indicating the likelihood that the modeled hydrogen distribution at solar maximum is closer to the actual distribution. This result is consistent with a higher fraction of satellite atoms being produced via evaporative processes at solar maximum. Charge exchange collisions with ionospheric-plasmaspheric ions play a larger role at solar minimum when exobase densities are higher [*Bishop*, 1991]. The larger slope in the ratio of the observed-to-calculated intensity versus shadow altitude at solar minimum is consistent with an underestimation of the satellite population in the evaporative exospheric model.

[33] Although more information is required to determine an appropriate choice of satellite parameters corresponding to the NRLMSISE-00 thermospheric conditions, the sensitivity studies presented here do provide insight regarding the upper atmospheric hydrogen density profile. When NRLMSISE-00 is used as the model thermosphere, the calculated intensities are brighter at solar maximum than at solar minimum irrespective of the choice of an evaporative exospheric extension or the option for satellite specific parameters accounting for charge exchange. The observed WHAM column emission intensities are brighter than are the calculated intensities in all cases, for both solar minimum and maximum conditions, and when either an evaporative exosphere or one with specified satellite parameters is used.

[34] All combinations of satellite parameters that we used resulted in a smaller slope in the ratio of the observed-to-calculated intensity versus shadow altitude than when the evaporative exospheric extension is used. When the evaporative exosphere model is used, the slope of the ratio of the observed-to-calculated intensities versus shadow altitude is greater at solar minimum; additionally there is more improvement in the slope with the use of satellite parameters for solar minimum conditions. These results are consistent with an underestimation of the satellite population in the evaporative model, likely due to not adequately accounting for satellite orbits created through charge exchange with warmer ions. The magnitude of the ratios of the observed-to-calculated intensities also appear to be improved with the satellite specific parameters. However, caution is warranted because additional sensitivity studies indicate that the

magnitude of the ratios is very sensitive to the choice of satellite density parameter (n_s).

[35] While our ratio approach does not retrieve the underlying hydrogen distribution, a review of past comparisons with MSIS suggests areas of agreement and difference with past results. Finding that the MSIS hydrogen distribution was inconsistent with observations, *Bishop* [2001] developed a three-component parametric model for hydrogen (mesospheric peak hydrogen density, the exobase hydrogen density, and hydrogen upward flux from the mesosphere) with densities near and below 120 km approximated by a Chapman layer, and above to the upper thermospheric boundary determined by the upward diffusive flux equation. The WHAM ratio comparisons presented here are consistent with previous studies in which the MSIS hydrogen density profile (MSIS90) has been shown to be lower throughout the thermosphere than the best fit hydrogen density profiles retrieved using forward modeling with the lyao_rt code for ground-based data taken during near-solar-minimum [*Bishop et al.*, 2001]. However, there is an apparent disagreement between the WHAM comparison and the hydrogen profile retrieved from the STP 78–1 Lyman α observations during near-solar-maximum conditions. The MSIS profile was of higher density throughout the thermosphere than that retrieved from the STP 78–1 observations [*Bishop*, 2001].

[36] In the *Bishop et al.* [2001] study, Fabry-Perot Balmer α observations taken in multiple viewing geometries from Haleakala during near-solar-minimum conditions in 1988 were used as constraints for forward modeling density retrievals using the three component thermospheric model, the analytic evaporative exosphere, and the lyao_rt code. The MSIS hydrogen profile was lower throughout the thermosphere than were the profiles retrieved via forward modeling fits to the Haleakala Fabry-Perot observations. *Bishop et al.* [2001] further conclude that the thermospheric hydrogen column abundance associated with the MSIS profile for solar minimum is too low by a factor of $\sim$2 compared to the column abundances corresponding to the profiles retrieved from the Haleakala observations.

[37] Near coincident satellite observations of the hydrogen Lyman β line and Wisconsin ground-based Fabry-Perot observations of Balmer α were used by *Bishop et al.* [2004] as constraints for forward modeling retrievals of best fit hydrogen densities during year 2000 solar maximum conditions. One of the best fit profiles was higher in density than the MSIS profile throughout the thermosphere to the exobase at which altitude the profiles were approximately coincident. However, the other candidate solutions had densities higher than MSIS throughout most of the thermosphere to an altitude of $\sim$300 km and then were lower than MSIS at altitudes above [*Bishop et al.*, 2004]. Additionally, *Bishop* [2001] used forward modeling to retrieve a best fit profile corresponding to the STP 78–1 near-solar-maximum Lyman α disk-to-limb scanning data. This profile fit however, was of lower density than MSIS throughout the thermosphere [*Bishop*, 2001].

[38] Although discrepancies were found between MSIS and previous observations, the WHAM comparison presented here is the first with observations taken by a single instrument during different phases of the solar cycle. Both the observed and calculated intensities are brighter during near-solar-maximum conditions over the entire shadow altitude range of the observations (see Figures 3 and 4). The line center solar Lyman β flux that excites geocoronal hydrogen varies by a factor of about two over the solar cycle, thus accounting for the brighter emission at solar maximum, even for shadow altitudes less than $\sim$1500 km where the hydrogen column density is lower at solar maximum than for solar minimum conditions (see Figure 6). As revealed by the larger magnitude and slope of the ratio of the calculated maximum to minimum intensity as a function of shadow altitude (see Figure 5), the solar cycle variation in the calculated intensities using the evaporative model is greater than that observed. Differences in the slopes of the observed and calculated ratios indicate discrepancies in the underlying hydrogen distributions, whereas differences in the magnitude of the solar cycle variation could also be due to uncertainties in calibration and solar excitation flux.

[39] Several factors likely contribute to the discrepancies in the model/data comparisons. The evaporative version of the *Bishop* [1991] analytic model does not account for differences in the temperatures of the ions and neutral atoms. Thus, the evaporative exosphere likely underestimates the contribution of charge exchange to the creation of satellite orbits with higher apogees. Regarding the thermosphere, hydrogen in the MSIS model is not assimilated from direct measurements of hydrogen densities, but rather is derived from charge exchange equilibrium analyses of Atmospheric Explorer observations of H^+, O^+, and O, and only for orbits above 250 km. Extrapolation to lower thermospheric altitudes assumes adjustments to diffusive equilibrium [*Brinton et al.*, 1975; *Breig et al.*, 1976; *Bishop*, 2001]; however, inclusion of the physics of diffusive flow was found to be of critical importance by *Bishop et al.* [2001, 2004] in improving forward model fits to observations via his three component thermospheric model. Additionally, the lyao_rt radiative transfer code assumes spherical symmetry [*Bishop*, 1999].

[40] Sources of observational uncertainty are reviewed by *Nossal et al.* [2008] and include the absolute intensity calibration and tropospheric scattering. The future use of an updated tropospheric scattering correction code is estimated to reduce the observed column emission intensity by 5–20%, depending upon the viewing geometry. The uncertainty in the WHAM absolute intensity calibration is $\pm$ 10% [*Nossal et al.*, 2008]. Errors in the intensity calibration and in the solar Lyman β line center excitation flux would be constant offsets and would not affect the slope of the ratio of the observed-to-calculated intensity versus shadow altitude.

[41] *Anderson et al.* [1987] used the Monte Carlo exospheric hydrogen profiles of *Tinsley et al.* [1986] and a radiative transfer code to predict intensities that would be observed from the ground from midlatitudes and obtained similar results to those we obtained with the lyao_rt radiative transfer code and the NRLMSISE-00 and *Bishop* [1991] analytic model exosphere density distribution. As in the case of the NRLMSISE-00 model extended with the *Bishop* [1991] exospheric analytic model, the *Tinsley et al.* [1986] hydrogen distribution generated using Monte Carlo modeling has higher hydrogen densities at solar minimum for altitudes less than about 6000 km. However, the *Tinsley et al.* [1986] densities are approximately constant over the solar cycle at higher exospheric altitudes. The nearly

constant hydrogen densities between about 2 R_E and 10 R_E in the Monte Carlo generated distribution is thought to be due to a relatively small solar cycle variation in the modeled ion temperature [*Tinsley et al.*, 1986]. The predicted column emission intensities calculated using the *Tinsley et al.* [1986] distributions were higher for solar maximum than for minimum conditions for most viewing geometries [*Anderson et al.*, 1987]. The solar cycle variation in the *Anderson et al.* [1987] modeling was also of larger magnitude than that observed in the Wisconsin solar cycles 21 and 22 observations [*Nossal et al.*, 1993].

9. Conclusions

[42] The high precision WHAM observations used together with the lyao_rt global resonance radiative transfer code provide a means for validation of the solar cycle variation in existing and future models of upper atmospheric hydrogen distributions. There is agreement between the observed and calculated intensities in that both are higher for solar maximum conditions for the viewing geometries corresponding to our observations. When the NRLMSISE-00 model is used to provide the thermospheric hydrogen distribution, background thermosphere, and the inputs to the *Bishop* [1991] evaporative analytic exosphere model, the calculated column intensities are lower than those observed for both solar minimum and maximum conditions. The differences in the slope of the intensity versus shadow altitude for the observed and calculated column emission intensity (as shown in Figures 4 and 5) cannot be reconciled with an adjusted offset due to uncertainties in the absolute intensity calibration or solar excitation flux, thus indicating differences in the underlying hydrogen distributions.

[43] The NRLMSISE-00 thermosphere and the *Bishop* [1991] analytic model exospheric extension both play important roles in determining the modeled upper atmospheric hydrogen distribution. While the evaporative extension of the *Bishop* [1991] analytic model uses inputs directly from NRLMSISE-00 to calculate the exospheric orbital populations, the model does not account for the warmer temperatures of the ions involved in charge exchange reactions with the neutral hydrogen atoms. The better model/data agreement near solar maximum and the improvement in the slope of the observed-to-calculated ratios with the use of satellite specific parameters are consistent with an underestimation of the population of satellite atoms at higher altitudes in the evaporative exospheric model. Furthermore, the lack of direct measurements of hydrogen and assumptions by MSIS of diffusive equilibrium may contribute to the differences in the column intensities calculated with NRLMSISE-00 and the *Bishop* [1991] analytic hydrogen distribution compared here with the WHAM observations. Discrepancies reported here between the observations and intensities calculated from existing models highlight the need for continued model development of the geocoronal hydrogen distribution extending from the thermosphere into the exosphere.

[44] **Acknowledgments.** We are grateful to the late James Bishop for many years of collaboration, the use of his lyao_rt code, and his invaluable insights regarding geocoronal science. The authors also thank the WHAM astronomical team, particularly Matt Haffner and Ron Reynolds. We also thank Carey Woodward and Jeff Percival for assistance with analysis. We appreciate helpful discussions with Geoff Crowley, Alan Burns, Stan Solomon and Liying Qian regarding modeling. In addition, we thank Doug Drob and John Emmert for assistance relating to NRLMSISE-00. We also greatly appreciate insightful comments from the reviewers. This research was supported by the National Science Foundation grants ATM-0334611, ATM-0836367, and AST-9619424.

[45] Philippa Browning thanks the reviewers for their assistance in evaluating this paper.

References

Anderson, D. E., Jr., R. R. Meier, R. R. Hodges Jr., and B. A. Tinsley (1987), Hydrogen Balmer alpha intensity distributions and line profiles from multiple scattering theory using realistic geocoronal models, *J. Geophys. Res.*, *92*, 7619–7642, doi:10.1029/JA092iA07p07619.

Bishop, J. (1985), Geocoronal structure: The effects of solar radiation pressure and the plasmaspheric interaction, *J. Geophys. Res.*, *90*, 5235–5245, doi:10.1029/JA090iA06p05235.

Bishop, J. (1991), Analytic exosphere models for geocoronal applications, *Planet. Space Sci.*, *39*, 885–893, doi:10.1016/0032-0633(91)90093-P.

Bishop, J. (1999), Transport of resonant atomic hydrogen emissions in the thermosphere and geocorona: Model descriptions and applications, *J. Quant. Spectrosc. Radiat. Transfer*, *61*, 473–491, doi:10.1016/S0022-4073(98)00031-4.

Bishop, J. (2001), Thermospheric atomic hydrogen densities and fluxes from dayside Lyman α measurements, *J. Atmos. Sol. Terr. Phys.*, *63*, 341–353, doi:10.1016/S1364-6826(00)00212-1.

Bishop, J., J. Harlander, S. Nossal, and F. L. Roesler (2001), Analysis of Balmer α intensity measurements near solar minimum, *J. Atmos. Sol. Terr. Phys.*, *63*, 331–340, doi:10.1016/S1364-6826(00)00211-X.

Bishop, J., E. J. Mierkiewicz, F. L. Roesler, J. F. Gomez, and C. Morales (2004), Data-model comparison search analysis of coincident PBO Balmer α, EURD Lyman β geocoronal measurements from March 2000, *J. Geophys. Res.*, *109*, A05307, doi:10.1029/2003JA010165.

Brasseur, G., and S. Solomon (2005), *Aeronomy of the Middle Atmosphere*, Springer, Dordrecht, Netherlands.

Breig, E. L., W. B. Hanson, and J. H. Hoffman (1976), In situ measurements of hydrogen concentration and flux between 160 and 300 km in the thermosphere, *J. Geophys. Res.*, *81*, 2677–2686, doi:10.1029/JA081i016p02677.

Brinton, H. C., H. G. Mayr, and W. E. Potter (1975), Winter bulge and diurnal variations in hydrogen inferred from AE-C composition measurements, *Geophys. Res. Lett.*, *2*, 389–392, doi:10.1029/GL002i009p00389.

Chamberlain, J. W. (1963), Planetary coronae and atmospheric evaporation, *Planet. Space Sci.*, *11*, 901–960, doi:10.1016/0032-0633(63)90122-3.

Chamberlain, J. W., and D. M. Hunten (1987), *Theory of Planetary Atmospheres: An Introduction to their Physics and Chemistry*, 2nd ed., Academic, San Diego, Calif.

Coakley, M. M., F. L. Roesler, R. J. Reynolds, and S. Nossal (1996), Fabry-Perot/CCD annular summing spectroscopy: Study and implementation for aeronomy applications, *Appl. Opt.*, *35*, 6479–6493, doi:10.1364/AO.35.006479.

Haffner, L. M., R. J. Reynolds, S. L. Tufte, G. J. Madsen, K. P. Jaehnig, and J. W. Percival (2003), The Wisconsin H-alpha mapper northern sky survey, *Astrophys. J.*, *149*, 405–422, doi:10.1086/378850.

Hedin, A. E. (1991), Extension of the MSIS thermosphere model into the middle and lower atmosphere, *J. Geophys. Res.*, *96*, 1159–1172, doi:10.1029/90JA02125.

Kerr, R. B., et al. (2001a), Periodic variations of geocoronal Balmer α brightness due to solar driven exospheric abundance variations, *J. Geophys. Res.*, *106*(A12), 28,797–28,817, doi:10.1029/1999JA900186.

Kerr, R. B., et al. (2001b), Secular variability of the geocoronal Balmer α brightness: Magnetic activity and possible human influences, *J. Geophys. Res.*, *106*(A12), 28,819–28,830, doi:10.1029/1999JA900187.

Leen, T. (1979), Application of radiative transfer theory to photometric studies of astronomical objects, MS thesis, Univ. of Wis.-Madison, Madison.

Meier, R. R. (1995), Solar Lyman-series line profiles and atomic hydrogen excitation rates, *Astrophys. J.*, *452*, 462–471, doi:10.1086/176318.

Meier, R. R. (1996), Solar Lyman-series line profiles and atomic hydrogen excitation rates: Erratum, *Astrophys. J.*, *468*, 455, doi:10.1086/177705.

Mierkiewicz, E. J., F. L. Roesler, S. M. Nossal, J. Bishop, R. J. Reynolds, and L. M. Haffner (2006), Geocoronal hydrogen studies using Fabry-Perot interferometers, Part 1: Instrumentation, observations, and analysis, *J. Atmos. Sol. Terr. Phys.*, *68*, 1520–1552.

Nossal, S., R. J. Reynolds, F. L. Roesler, and F. Scherb (1993), Solar cycle variations of geocoronal Balmer α emission, *J. Geophys. Res.*, *98*, 3669–3676, doi:10.1029/92JA02568.

Nossal, S., F. L. Roesler, R. J. Reynolds, M. Haffner, S. Tufte, J. Bishop, and J. Percival (2001), Geocoronal Balmer α intensity measurements using

the WHAM Fabry-Perot facility, *J. Geophys. Res.*, *106*, 5605–5616, doi:10.1029/2000JA000003.

Nossal, S. M., F. L. Roesler, E. J. Mierkiewicz, and R. J. Reynolds (2004), Observations of solar cyclical variations in geocoronal Hα column emission intensities, *Geophys. Res. Lett.*, *31*, L06110, doi:10.1029/2003GL018729.

Nossal, S. M., E. J. Mierkiewicz, F. L. Roesler, R. J. Reynolds, and L. M. Haffner (2006), Geocoronal hydrogen studies using Fabry-Perot interferometers, Part 2: Long term observations, *J. Atmos. Sol. Terr. Phys.*, *68*, 1553–1575, doi:10.1016/j.jastp.2005.08.025.

Nossal, S. M., E. J. Mierkiewicz, F. L. Roesler, L. M. Haffner, R. J. Reynolds, and R. C. Woodward (2008), Geocoronal hydrogen observations spanning three solar minima, *J. Geophys. Res.*, *113*, A11307, doi:10.1029/2008JA013380.

Picone, J. M., A. E. Hedin, and D. P. Drob (2002), NRLMSISE-00 empirical model of the atmosphere: Statistical comparisons and scientific issues, *J. Geophys. Res.*, *107*(A12), 1468, doi:10.1029/2002JA009430.

Reynolds, R. J., F. L. Roesler, F. Scherb, and J. Harlander (1990), Fabry-Perot/CCD multi-channel spectrometer for the study of warm, ionized interstellar gas and extragalactic clouds, in *Instrumentation in Astronomy VII*, *Proc. SPIE Int. Soc. Opt. Eng.*, *1235*, 610.

Scherb, F. (1981), Hydrogen production rates from ground-based Fabry-Perot observations of comet Kohoutek, *Astrophys. J.*, *243*, 644, doi:10.1086/158630.

Tinsley, B. A., R. R. Hodges Jr., and R. P. Rohrbaugh (1986), Monte Carlo models for the terrestrial exosphere over a solar cycle, *J. Geophys. Res.*, *91*, 13,631–13,647, doi:10.1029/JA091iA12p13631.

Warren, H. P., J. T. Mariska, and K. Wilhelm (1998), High-resolution observations of the Solar hydrogen Lyman lines in the quiet sun with the SUMER instrument on SOHO, *Astrophys. J. Suppl. Ser.*, *119*, 105–120, doi:10.1086/313151.

E. J. Mierkiewicz, S. M. Nossal, and F. L. Roesler, Department of Physics, University of Wisconsin-Madison, 1150 University Ave., Madison, WI 53706, USA. (emierk@astro.wisc.edu; nossal@physics.wisc.edu; roesler@physics.wisc.edu)